Stray Flux Monitoring for Reliable Detection of Rotor Faults under the Influence of Rotor Axial Air Ducts

Park, Y., Yang, C., Kim, J., Kim, H., Lee, S.B., Gyftakis, K.N., Panagiotou, P., Kia, S.H. and Capolino, G.A

Original citation & hyperlink:
Park, Yonghyun, et al. "Stray Flux Monitoring for Reliable Detection of Rotor Faults under the Influence of Rotor Axial Air Ducts." *IEEE Transactions on Industrial Electronics* (2018).
https://dx.doi.org/10.1109/TIE.2018.2880670

ISSN: 0278-0046

Publisher: IEEE

Stray Flux Monitoring for Reliable Detection of Rotor Faults under the Influence of Rotor Axial Air Ducts

***Abstract*—Monitoring of induction motor faults based on stray flux measurement has been investigated by many researchers due to its potential benefits in cost and simplicity. Although it was shown that flux based monitoring can provide sensitive fault detection comparable to that of motor current signature analysis (MCSA), the lack of "remote" monitoring capability has limited its practical use. The performance and reliability of stray flux-based detection of induction motor rotor cage faults is evaluated in this paper. It is shown for the first time in this work that spectrum analysis of the radial stray flux can provide reliable detection of rotor faults immune to the influence of rotor axial air ducts, which is the most common cause of false rotor fault alarms. The reliability and sensitivity of stray flux based rotor fault detection is demonstrated through experimental testing on laboratory and 6.6 kV field motors.**

***Index Terms*—Electrical Fault Detection, False Alarms, Fault Diagnosis, Motor Current Signature Analysis (MCSA), Flux Signature Analysis, Induction Motor, Stray flux, Rotor Fault, Spectral Analysis.**

I. Introduction

THE bar or end ring of the rotor cage of induction motors is known to be vulnerable to failure in applications with frequent motor starts/stops and/or excessive load torque variations. Although a motor with rotor cage damage operates with increased low frequency torque pulsations and vibration, it can continue to operate without interrupting the driven process. The main purpose of detecting rotor faults is to prevent secondary damage that can be caused by 1) arcing between the loose bar and rotor core that results in permanent core damage or 2) protrusion of the bar or its segments into the airgap or stator that can cause forced outage of the motor and driven process. Many off-line tests and on-line monitoring methods have been developed and applied to detection of rotor faults. Majority of the research effort from the academic community for monitoring of rotor condition was on on-line test methods based on the current, vibration, flux, or speed measurements [1]-[2].

Motor current signature analysis (MCSA) is currently the most commonly applied means of detecting faults in the rotor cage of induction machines while the motor is in service. Its remote monitoring capability from the motor control center using existing current transformers makes it an attractive tool for monitoring medium-high voltage motors operating in the field. There are numerous publications that show the fault detection capability of MCSA for preventing secondary motor damage due to rotor cage failure [1]-[6]. One of the main concerns of applying MCSA in the field is the false indications that are occasionally produced. It has been reported that false MCSA indications can be produced by magnetic asymmetry in the rotor structure, load variations, broken outer cage bars in double cage rotors, manufacturing imperfections, or non-adjacent bar damage [6]-[10]. The most common false MCSA indication produced in the field is caused by interference due to rotor axial cooling air ducts. The consequences of a false indication can be significant, as it can result in unnecessary rotor inspection (false positive) and/or forced outage of the motor and industrial process (false negative).

This has triggered active research on finding alternative solutions for reliable detection of rotor faults under the influence of axial ducts. The methods immune to the axial duct have limitations in that they require testing under conditions where penetration of flux in the rotor yoke is limited. In [9] and [11], it is shown that fault detection is independent of axial ducts when testing is performed under standstill or startup conditions when flux cannot reach the axial ducts due to high slip. The limitation is that off-line standstill or motor startup testing cannot be performed frequently for applications where the motor is run continuously. It is shown in [13] that the space harmonics induced rotor fault components can be monitored for rotor fault detection independent of axial ducts; however, the sensitivity depends heavily on the stator winding design. It is also possible to distinguish between a rotor fault and axial duct influence if data measurement under two different load conditions is available [9]-[10]. However, this cannot be applied for applications operated under similar load conditions.

In this paper, radial stray flux spectrum analysis is proposed as an alternative means of reliable and sensitive detection of rotor faults under steady state operation. It is shown for the first time in this work that radial flux monitoring can provide reliable indication of rotor faults, for cases where MCSA fails due to rotor axial duct interference. It is also shown that a low-cost flux coil installed on the surface of the motor frame can provide sensitive detection of rotor faults. The low cost, sensitive, and reliable fault detection capability of stray flux monitoring is demonstrated through experimental testing on laboratory and 6.6 kV field motors.

II. Radial Stray Flux Monitoring

The concept of using axial, radial, or circumferential flux measurements obtained from internal or external flux sensors for detecting electric machine faults has been studied since the 1980s [14]-[25]. The main motivation behind the investigation

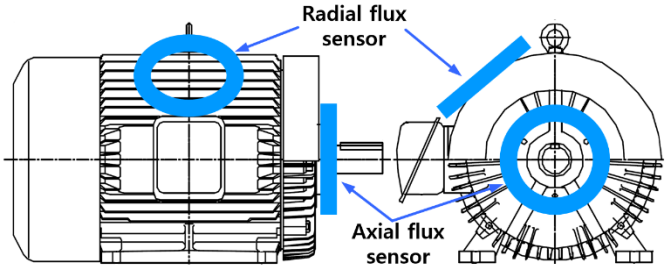

Fig. 1. Axial and radial stray flux sensors

of flux based fault detection was the low cost, simplicity, and flexibility of flux measurement. External flux coils can be retrofit to motors operating in the field since they can be easily installed on the surface of the motor frame. It is shown in [14]-[16] that the axial stray (leakage) flux measured with a coil wound around the rotor shaft, as shown in Fig. 1, can be used to detect stator inter-turn, broken rotor bar, eccentricity, bearing faults, or supply voltage unbalance. Measurement of the radial stray (leakage) flux on the motor frame [16]-[25], as shown in Fig. 1, and/or radial flux in the airgap [21]-[22] were studied for detection of broken rotor bars, mixed eccentricity, stator inter-turn, or bearing faults in induction motors. When the radial stray flux is measured at the surface of the stator frame, it measures the leakage component of the flux produced by the stator and rotor current. According to [19]-[20], the influence of the stator current produced flux is prevalent, and therefore, the radial stray flux sensor measurement contains information similar to that of the stator current. In [21], it is shown that external radial stray flux analysis can provide detection of rotor faults with sensitivity comparable or superior to internal stray flux, current, vibration, or torque spectrum analysis. An extensive survey of stray flux based detection of induction motor faults is presented in [16]. The main focus of the prior work on flux monitoring is on the detectability and sensitivity, and none of the papers investigate the reliability aspects as in this paper.

Despite the cost and sensitivity advantages of flux-based motor fault detection reported in the literature, it was not as well-received in the field as MCSA, mainly because access to the motor is required for installation of the flux sensor. Remote monitoring of motor faults is an important requirement in the field since data measurement in the motor control center is safe, clean, and convenient. This is more critical in industries where large quantity of motors is operated in a hostile environment, since the maintenance engineers performing walk-around inspection are exposed to safety risks, and permanent installation of sensors is not desirable.

Although access to the motor is required for walk-around type monitoring or permanent sensor installation for flux based monitoring, it can be justified if it can provide reliable monitoring of motor faults for cases where on-line MCSA fails. The reliability of fault detection is a requirement that precedes the remote monitoring capability due to the consequences associated with false positive or negative indications. In [25], it is shown that the influence of rotor cage faults and load torque oscillations can be separated with radial stray flux monitoring for reliable fault detection. In this work, flux based monitoring is studied for reliable detection of rotor faults in the presence of magnetic rotor asymmetry, which is the most common cause of false MCSA indication. Radial stray flux measurement is considered in this paper, since it is easier to implement or retrofit compared to axial or internal flux measurement. Leakage flux in the radial direction can also be measured with higher sensitivity compared to the axial direction since the leakage flux is measured closer to the main flux path.

III. False MCSA Rotor Fault Indications Produced by Axial Air Ducts

The axial cooling duct structure, shown in Fig. 2, provides cooling of the rotor with axial air flow, and energy/cost savings since the rotational inertia can be reduced with a lighter rotor. Axial ducts are employed in the rotor of most medium-high voltage motors due to these benefits. It is shown in [6]-[13] that false positive and negative MCSA indications can be produced if the number of axial ducts is identical to the number of poles. This is the leading root cause of false MCSA rotor fault indications in the field. Axial ducts can cause the magnetic flux path to be asymmetric depending on the relative position between the rotor and rotating field, as illustrated in Fig. 3. Flux is not present behind the ducts in Fig. 3(a), whereas it penetrates behind the ducts in Fig. 3(b). This leads to variation in the

Fig. 2. 6.6 kV, 280 kW, 4 pole induction motor with 4 axial cooling ducts

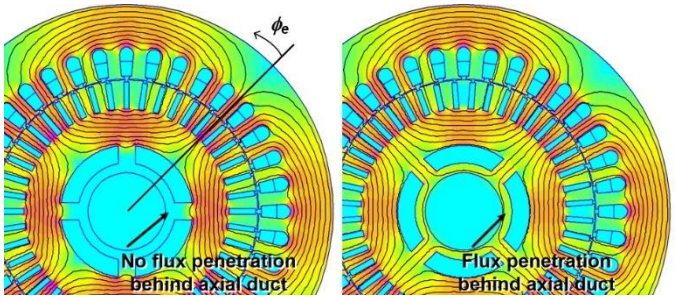

(a) (b)

Fig. 3. Flux distribution in 4 pole motor with 4 axial air ducts when magnetic poles and duct arms are (a) not aligned and (b) aligned under steady-state operation (angle ϕ_e defined)

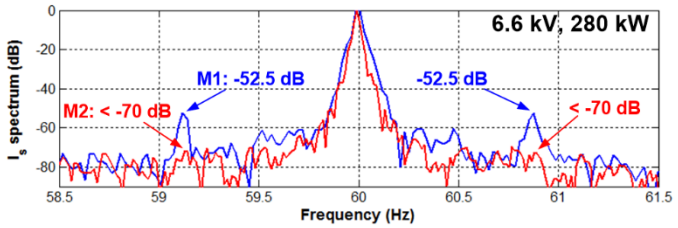

Fig. 4. Stator current spectrum of two 6.6 kV, 280 V motors (4 pole, 4 axial ducts) shown in Fig. 1 with (M1) and without (M2) false rotor fault alarm (1/45 Hz frequency resolution)

equivalent magnetizing inductance, L_m, and stator current in a way similar to that of a rotor cage fault. If the number of air ducts and poles are the same, this results in induction of a frequency component in the stator current that is identical to that of rotor faults given by

$$f_{rf} = (1 \pm 2ks)f_s, \tag{1}$$

where f_s is the fundamental frequency of the supply, s is the slip, and k is a positive integer [10]-[13]. This frequency component induced in the stator current by axial air duct influence can be misinterpreted as a rotor fault.

The results of MCSA performed on two identical 6.6 kV, 280 kW, 4 pole motors M1 and M2 (Fig. 1) with 4 axial ducts operating under the same load condition are shown in Fig 4. It can be seen that the f_{rf} component of M1 is high enough (−52.5 dB) to suspect a rotor fault, whereas it is very low at ≤−70 dB for M2. The difference in the degree of magnetic asymmetry caused by axial ducts can attributed to part-to-part variation introduced in the rotor due to component and manufacturing tolerances [11]-[13]. Inspection of the motor with the higher f_{rf} component showed that the rotor cage was in good condition for both M1 and M2, and it was concluded that a false alarm was produced by MCSA due to axial air ducts.

The principle behind induction of the (1-2s)f_s components in the stator current due to axial ducts and rotor cage faults can be described from the simplified per phase "steady state" electrical equivalent circuit shown in Fig. 5 [11]. If the number of air ducts and poles are equal, the per phase equivalent magnetizing reactance, x_m, seen from the fixed stator winding fluctuates due to the asymmetric flux path (Fig. 3). The fluctuation in x_m is at twice the rotor electrical speed, (1-s)ω_s, given by

$$x_m = X_{m0} - \Delta X_m \cos(2(1-s)\omega_s t), \tag{2}$$

where ω_s is the supply frequency in *rad*/*s*, and X_{m0}, ΔX_m represent the average and peak to peak variation in x_m, respectively. Similarly, if a rotor cage fault due to a broken bar or end ring is present, the equivalent rotor resistance, r_r, seen from the stator winding also fluctuates at twice the rotor speed as

$$r_r = R_{r0} - \Delta R_r \cos(2(1-s)\omega_s t - 2\phi_e), \tag{3}$$

where R_{r0}, ΔR_r are the average and peak to peak variation of r_r, respectively. ϕ_e is the electrical angle of the broken rotor bar with respect to the center of the air duct, as shown in Fig. 3(a). The variation in the impedances with rotor position was taken into account in the steady state analysis, and the phase angle is defined only for r_r since it the relative angle between the two components that is of interest. The equivalent rotor leakage inductance, x_{lr}, also changes with rotor cage damage, but is neglected in the analysis here since x_{lr} is negligibly small compared to r_r/s in steady state. The stator equivalent resistance, r_s, and leakage inductance, x_{ls}, are also neglected in the analysis for simplicity. It is more convenient to obtain expressions for the stator, magnetizing, and rotor currents, I_s, I_m, and I_r, using the admittance, y_m, and conductance, g_r, given by the reciprocal of x_m and r_r, respectively, as

$$y_m = 1/x_m \approx Y_{m0} + \Delta Y_m \cos(2(1-s)\omega_s t), \tag{4}$$

$$g_r = 1/r_r \approx G_{r0} + \Delta G_r \cos(2(1-s)\omega_s t - 2\phi_e), \tag{5}$$

where Y_{m0}, ΔY_m, (and G_{r0}, ΔG_r) represent the average and peak to peak variation of y_m (and g_r).

Expressions for i_s, i_m, and i_r can be derived from (4), (5), the equivalent circuit (Fig. 5) and the stator voltage given by

$$v_s = V_s \cos(\omega_s t), \tag{6}$$

where V_s is the peak value of the voltage. It can be shown that i_s can be derived from the sum of i_m and i_r as

$$\begin{aligned} i_s = i_m + i_r &= v_s(-jy_m + g_r s) \\ &= V_s(Y_{m0} \sin\omega_s t + G_{r0} s \cos\omega_s t) \\ &+ \frac{V_s}{2}\left[\begin{matrix} \Delta Y_m \sin(1-2s)\omega_s t + \Delta G_r s \cos\{(1-2s)\omega_s t - 2\phi_e\} \\ +\Delta Y_m \sin(3-2s)\omega_s t + \Delta G_r s \cos\{(3-2s)\omega_s t - 2\phi_e\} \end{matrix}\right] \end{aligned} \tag{7}$$

This equation shows that the variation in x_m due to axial air ducts and variation in r_r due to rotor faults produce identical (1-2s)f_s components in the stator current. The (1-2s)f_s component in the stator current, denoted as subscript 1-2s, can be expressed as the magnetizing and rotor current components as

$$\begin{aligned} i_{s,1-2s} = i_{m,1-2s} + i_{r,1-2s} = I_{m,1-2s} \sin(1-2s)\omega_s t + \\ I_{r,1-2s} s \cos\{(1-2s)\omega_s t - 2\phi_e\}, \end{aligned} \tag{8}$$

where $I_{m,1-2s}$, $I_{r,1-2s}$ are $V_s\Delta Y_m/2$, $V_s\Delta G_r/2$, respectively. From (8), the amplitude of the (1-2s)f_s component of i_s, $I_{s,1-2s}$ can be derived as a function of $I_{m,1-2s}$ and $I_{r,1-2s}$ as

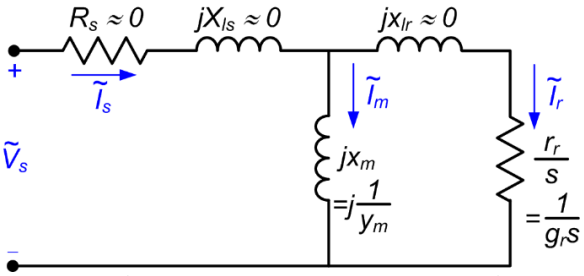

Fig. 5. Simplified per phase electrical equivalent circuit of induction motor for describing interaction between axial air duct- and rotor fault-induced components in MCSA

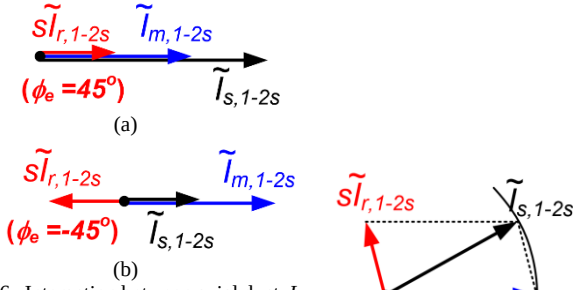

Fig. 6. Interaction between axial duct, $I_{m,1-2}$ ponents for different values of ϕ_e (assumption $I_{m,1}$ ases of $I_{m,1-2s}$ and $sI_{r,1-2s}$ interactions: (a) maximum $I_{s,1-2s}$ (in phase, ϕ_e=-45°), (b) minimum $I_{s,1-2s}$ (out of phase, ϕ_e=-45°), (c) no change in $I_{s,1-2s}$ (ϕ_e=-7.25°).

$$I_{s,1-2s} = \sqrt{I_{m,1-2s}^2 + 2I_{m,1-2s}I_{r,1-2s}\, s \sin 2\phi_e + I_{r,1-2s}^2 s^2}. \quad (9)$$

This equation clearly shows that the f_{rf}=(1-2s)f_s component of the stator current monitored for rotor fault detection can be produced by a combination of axial ducts and rotor cage faults. The amplitude of the f_{rf} component depends on the amplitudes of $I_{m,1\text{-}2s}$, $I_{r,1\text{-}2s}$, and the position of the rotor fault, ϕ_e. The two components are in phase (additive), if the rotor fault is located at ϕ_e=45° and out of phase (subtractive), if located at ϕ_e=-45°, as can be seen in (8)-(9). An example of the case where the two components are in phase to produce maximum $I_{s,1\text{-}2s}$ is shown in Fig. 6(a). It is assumed here that the amplitude of $sI_{r,1\text{-}2s}$ is half of $I_{m,1\text{-}2s}$ at a given slip for simplicity of illustration. The case where the two components are out of phase to produce minimum $I_{s,1\text{-}2s}$ is shown in Fig. 6(b). This shows that a rotor fault of the same severity can cause the $I_{s,1\text{-}2s}$ component to either increase or decrease depending on the location of the fault, ϕ_e. It is also possible for the rotor fault to be not noticeable at all as it does not cause any change in the amplitude of the $I_{s,1\text{-}2s}$ component. It can be seen from (8)-(9) that this condition occurs at ϕ_e=-7.25° for this particular case, as shown in Fig. 6(c). Fig. 6 and (9) clearly show that the interaction between the axial duct and rotor fault components can produce false positive or negative MCSA rotor fault indications.

It is very difficult to screen out false indications with MCSA since the number of air ducts is usually unknown and the rotor fault location, ϕ_e, is random. Investigation of alternative test methods showed that rotor faults can be detected reliably independent of the axial duct influence, if testing is performed at high rotor slip. Penetration of the flux into the rotor yoke or behind ducts is limited at high slip due to eddy current rejection of the rotor cage, and therefore, testing under standstill or the startup transient is not influenced by the axial ducts. However, assembled standstill testing such as the single phase rotation test [26] requires manual rotation of the rotor in discrete steps, which could be difficult depending on the motor, load, or environment. Startup testing is not always feasible for motors that are operated continuously for long intervals or motors with short startup time, and is not desirable due to the startup stresses on the motor.

IV. Immunity of Radial Stray Flux Monitoring to Axial Air Duct Influence

The MCSA measurements on the 6.6 kV motor shown in Fig. 4 and the analysis provided in III show that the axial ducts and rotor faults can produce (1-2s)f_s components of comparable amplitude. This causes false fault indications and makes reliable rotor fault detection difficult with MCSA [9]. Investigation of alternative test methods show that off-line or startup testing have many limitations for application in the field. Since an on-line test method for rotor fault testing immune to the axial duct influence is highly desirable, justification behind radial stray flux based detection is presented in this section. The results of laboratory testing under carefully controlled conditions is given to show that radial flux measurement can provide sensitive detection of rotor faults while being insensitive to the axial air duct influence.

Radial stray flux measurement is a complex phenomenon as it is produced by a combination of the axial, radial, and circumferential leakage flux components [15]-[16], [24]. Stray flux produced by non-ideal asymmetries in the motor magnetic structure further complicates the problem [27]. Considering the complexity and difficulty of the problem, it is a non-trivial task to derive analytical equations or to perform a 3 dimensional finite element analysis to predict stray flux behavior with high precision. It is shown in many resources that the flux components are mainly produced by the stator current, and therefore, contains spectral components similar to that of the stator current [19]-[20]. The main principle behind the induction of the 2sf_s sideband components, f_{rf}, in the stray flux is similar to that of how they are induced in the stator current shown in III. A 'qualitative' explanation on how the f_{rf} components in the magnetic flux are produced by the MMF and magnetic reluctance variation can be given from a simplified equivalent magnetic circuit analysis. The magneto-motive force (MMF) produced by the stator current at f_s is modulated by the variation in the magnetic reluctance at 2(1-s)f_s due to axial air ducts and rotor cage damage, and this produces (1-2s)f_s components in the stray flux measurements. The magnetic reluctance fluctuates due to the varying magnetic flux paths with axial ducts. The change in magnetic reluctance is small since a high reluctance path is added to the main flux path when flux penetrates behind the ducts, as shown in Fig. 3(b). Similarly, the 'effective' magnetic reluctance changes

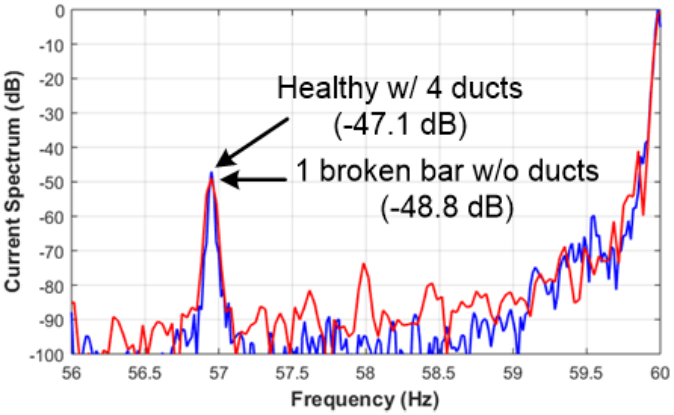

Fig. 7. Current spectra obtained from 380 V, 5.5 kW, 4 pole lab motor rotor with 4 axial ducts and no broken bars (case A) and rotor with no axial air ducts and 1 broken bar (case B)

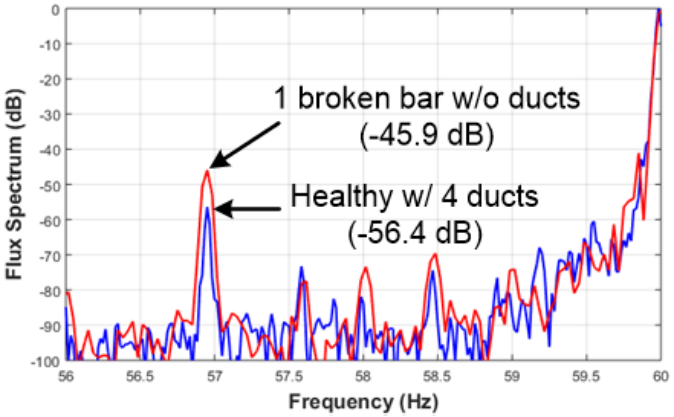

Fig. 8 Flux spectra obtained from 380 V lab , 5.5 kW, 4 pole motor rotor with 4 axial ducts and no broken bars (case A) and rotor with no axial air ducts and 1 broken bar (case B)

depending on rotor position due to change in the degree of cage eddy current rejection, if a broken rotor bar is present. The change in 'effective' magnetic reluctance is relatively larger when rotor faults are present than that produced by axial ducts.

Since analytic prediction of the radial stray flux measurement with high precision is difficult, the most effective and accurate means of demonstrating the relative difference in the amplitude of the f_{rf} components of flux is through a controlled laboratory test. The f_{rf} component of the stray flux can be compared for two cases, where the amplitude of the $(1\text{-}2s)f_s$ components in the stator current, $i_{s,1\text{-}2s}$, due to axial ducts alone, $i_{m,1\text{-}2s}$, and rotor fault alone, $i_{r,1\text{-}2s}$, are identical. The first test (case A) is performed on a healthy motor with no broken bars ($i_{r,1\text{-}2s}$=0), where $i_{s,1\text{-}2s}$ is produced by the axial ducts ($i_{m,1\text{-}2s}\neq 0$) only. The second test (case B) is performed on a motor without axial ducts ($i_{m,1\text{-}2s}$ =0), and with a rotor fault ($i_{r,1\text{-}2s}\neq 0$). Only the $(1+2s)f_s$ component was observed since the $(1+2s)f_s$ component is attenuated due to inertia. The tests were performed on a 380 V, 5.5 kW 4 pole motor with two rotor samples prepared for cases A and B. The axial duct dimensions and broken bar severity were carefully controlled so that the amplitude of the stator current $(1\text{-}2s)f_s$ components ($i_{s,1\text{-}2s}$) are similar for the two cases. The details on the rotor with axial duct and broken bar are given in detail in V.A.

The frequency spectra of the stator current and radial stray flux obtained with the two rotors with 1) 4 axial air ducts with no rotor fault (case A) and 2) rotor faults with no axial ducts (case B) are shown in Figs. 7-8, respectively. It can be seen in Fig. 7 that the $(1\text{-}2s)f_s$ components in the stator current are similar at -47.1 dB and -48.8 dB for cases A and B, respectively. Fig 8 shows that the $(1\text{-}2s)f_s$ components in the flux spectrum is significantly larger for the case of rotor faults (case B) when compared to the case of axial ducts (case A). The difference in the f_{rf} component in the flux measurement is 10.5 dB, for the two cases where the f_{rf} components are similar in the current spectrum. The f_{rf} component in the current spectrum is actually slightly lower for case B for which the f_{rf} component in the flux spectrum is much higher. This shows that the f_{rf} component in the radial stray flux spectrum is sensitive to rotor faults, while being insensitive to the influence of axial air ducts. This clearly shows that radial stray flux monitoring can provide reliable detection of rotor faults.

V. Experimental Study

A. Experimental Setup

An experimental study was performed to verify the claims made in this paper on the reliability benefits of radial stray flux based rotor fault detection. Experimental measurements of the radial stray flux were obtained on a 380 V, 5.5 kW, 1740 rpm, 4 pole motor in the laboratory, and on a 6.6 kV 280 kW, 4 pole motor (M1-M2, Fig. 1) in the field (both motors have 4 axial ducts). To test the reliability of radial stray flux spectrum analysis under controlled conditions of rotor fault and axial air duct interference, 4 axial ducts were created in the rotor of the laboratory motor. 20 small holes were drilled in 4 groups to create 4 axial ducts in the yoke of the 44 slot rotor, as shown in Fig. 9.

Artificial rotor cage fault conditions were produced by disconnecting the contact between the rotor bar and end ring joint. It is not possible to break bars at the exact $\phi_e = +45^o$ and -45^o locations (mechanical angle at $\pm 22.5^o$ with respect to the center of the duct) for this 44 slot 4 pole motor. 0, 1, and 2 rotor bars were broken as close as possible to the $\phi_e = +45^o$ and -45^o locations. These are the two extreme conditions where the rotor fault and axial duct influence on the $(1\text{-}2s)f_s$ component in the stator current add and cancel. When testing under faulty rotor conditions with the fault located at $\phi_e = 45^o$, the rotor was rotated in the direction of positive ϕ_e to obtain results with the rotor fault located at $\phi_e = 45^o$. To perform the tests with the fault located at $\phi_e = -45^o$, data was obtained with the same rotor rotated in the opposite direction instead of using another rotor.

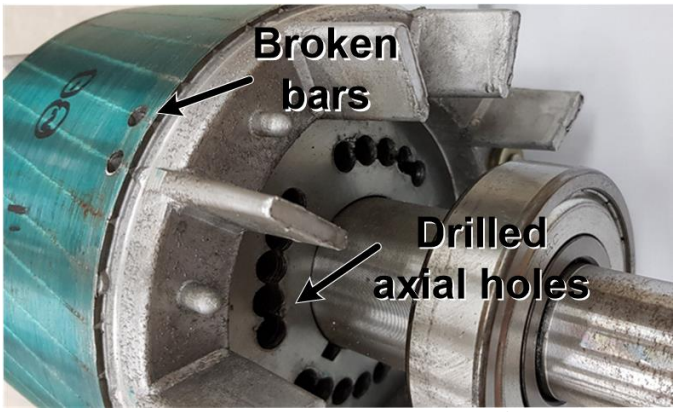

Fig. 9. 4 axial air ducts drilled in aluminum die cast rotor of 4 poles, 380 V, 5.5 kW induction motor


Fig. 10. Measurement of radial stray flux on 380 V, 5.5 kW, 4 pole lab motor

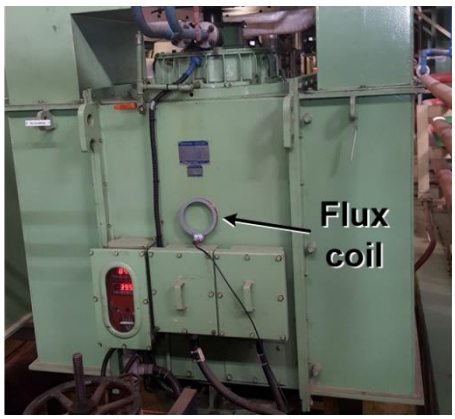

Fig. 11. Measurement of radial stray flux of 6.6 kV, 280 kW 4 pole pump motor with 4 axial air ducts

The stator current and radial stray flux were both measured for comparison under steady state motor operation with commercial sensors and a 16 bit data acquisition system. A 320 turn Helmholtz coil with 121 cm inner diameter and 155 cm outer diameter was used to measure the radial stray flux by placing it on the axial center of the motor frame, as shown in Fig. 10. 60 secs of data were acquired at 6 kHz sampling for a frequency resolution of 1/60 Hz. A Hanning window was applied to the flux and current data before the FFT operation, as this is most commonly used in commercial MCSA products. The load of the motor was set at 50%, 75%, and 100% rated load conditions since spectrum analysis for rotor fault detection is typically applied once or twice a year when the load is above 50% rated load to guarantee sensitive fault detection. Load was controlled by adjusting the field voltage of a 22.5 kW dc generator directly coupled to the motor.

Testing was also performed on the 6.6 kV, 280 kW, 4 pole motors, shown in Fig. 2, for which MCSA produced a false alarm due to axial ducts. Data was obtained from two identical vertical motors, M1 and M2 , sharing the load of condensate extraction pumps at a power generation facility. The current and stray flux measurements were obtained from the motors and analyzed for comparison. The radial stray flux was measured on the surface of the motor by placing the same flux sensor used for the lab motor on the axial center of the motor surface, as shown in Fig. 11.

B. Experimental Results – 380 V, 5.5 kW Lab Motor

Current- and flux-spectra analysis were performed on the lab motor under 50%, 75%, and 100% rated load conditions with 0, 1, and 2 broken rotor bars located at ϕ_e = +45° and -45° locations. The 36 different cases of current and flux measurements obtained for different load, fault severity and location, are shown in Figs. 12-15. The spectra of the stator current near f_s obtained with 0, 1, 2 broken bars located close to ϕ_e = -45° under 75% rated load are shown in Fig. 12 to show the case where MCSA can fail due to axial duct influence. It can be seen that the f_{rf} component is large at -47.1 dB when the motor is healthy due to the influence of the rotor axial ducts. Motors with healthy rotors typically produce an f_{rf} component below -60 dB. When the test was repeated with 1 broken bar, the f_{rf} component decreased to -58.2 dB. This value typically measured with a healthy rotor is produced because the rotor fault and axial duct induced components at $(1\text{-}2s)f_s$ are out of phase and cancel out. When 2 bars are broken, the f_{rf} components increases again to a high value of -42.8 dB because the rotor fault component dominates over that of the axial duct induced component. The results of Fig. 12 clearly demonstrates an example of MCSA failure due to the axial duct influence causing potential false positive (healthy) and false negative (1 broken bar) indications.

The MCSA measurements of the f_{rf} components for all conditions of different load and fault severity are shown in Fig. 13(a)-(b) for when fault is located close to ϕ_e = +45° and -45°., respectively. The results for the case of Fig. 12 are highlighted in Fig. 13(b). It can be seen in Fig. 13 that the baseline value of the f_{rf} component for a healthy motor is high due to the axial duct influence, and increases as the fault severity is increased for the case when the fault is close to ϕ_e = +45° because the fault and duct induced components are in phase. For the case where the fault is located close to ϕ_e = -45°, the f_{rf} component decreases with 1 broken bar and then either decreases or increases depending on the load when 2 bars are broken. This is because the fault and duct induced components are out phase. It is clear from the results of Figs. 12-13 that MCSA is not a reliable test that can potentially produce false positive and negative indications due to axial duct influence.

The results of the flux spectra and f_{rf} components obtained under identical conditions as Figs. 12 and 13 are shown in Figs. 14 and 15, respectively. The results of Fig. 14 show that the f_{rf} component is low at -56.4 dB for a healthy motor and shows a

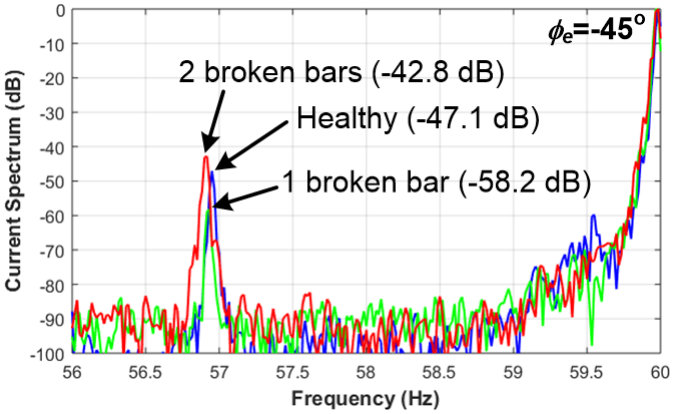

Fig. 12. MCSA results: $(1\text{-}2s)f_s$ component for laboratory motor with 0, 1, 2 of 44 broken bars located close to ϕ_e = -45° under 75% rated load conditions (normalized to f_s component)

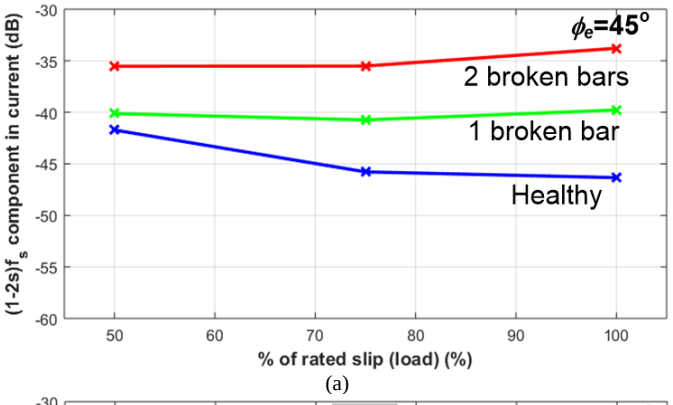

(a)

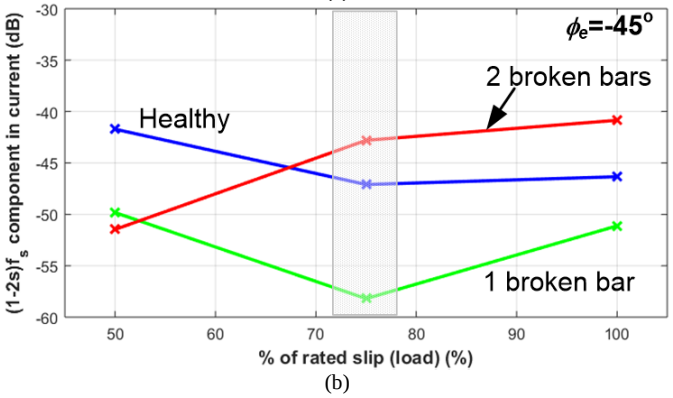

(b)

Fig. 13 MCSA results of $(1\text{-}2s)f_s$ component motor with 0, 1, 2 of 44 broken bars close to (a) ϕ_e=45° and (b) ϕ_e=-45° under 50, 75, 100% rated load conditions (normalized to f_s component)

significant and clear increase to -41.7 and -38.1 dB with 1 and 2 broken bars, respectively, under 75% rated load with the fault located close to ϕ_e = -45º. The results clearly demonstrate that rotor faults can be detected reliably regardless of the axial duct influence, for cases when MCSA produces false positive and negative indications (Fig. 12). The results obtained for the different load and fault severity conditions shown in Fig. 15(a)-(b) confirm that radial stray flux can provide sensitive detection of rotor faults for under different load conditions independent of the influence of axial ducts, as claimed in this paper. This can be attributed to the relatively high magnetic reluctance of the axial duct flux path making the change in the stray flux relatively small for the same stator MMF level, as described in IV. It can also be seen in Figs. 15(a)-(b) that the

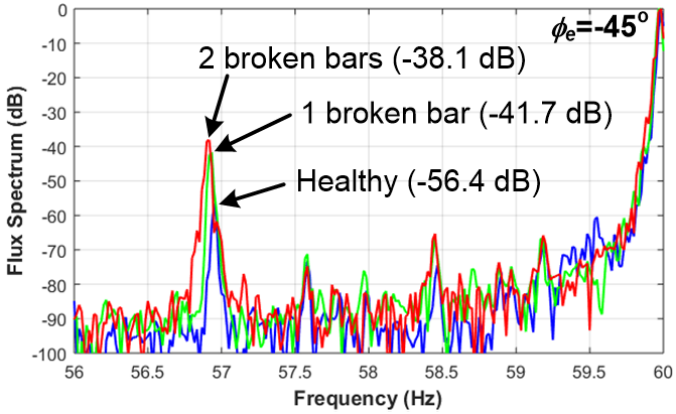

Fig. 14. Flux spectra: (1-2*s*)f_s component for laboratory motor with 0, 1, 2 of 44 broken bars at located close to ϕ_e = -45º under 75% rated load conditions (normalized to f_s component)

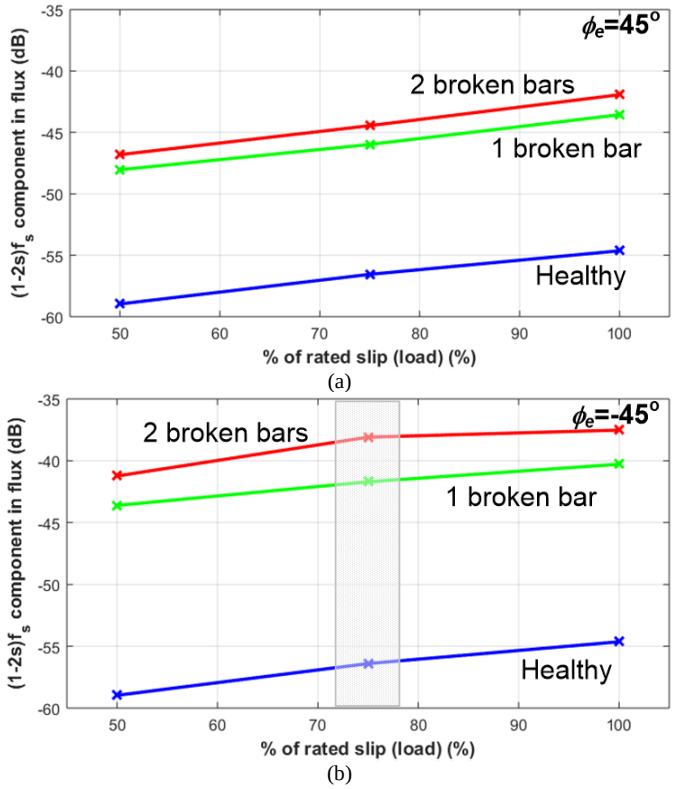

Fig. 15. Flux analysis results of (1-2*s*)f_s component motor with 0, 1, 2 of 44 broken bars close to (a) ϕ_e=45º and (b) ϕ_e=-45º under 50, 75, 100% rated load conditions (normalized to f_s component)

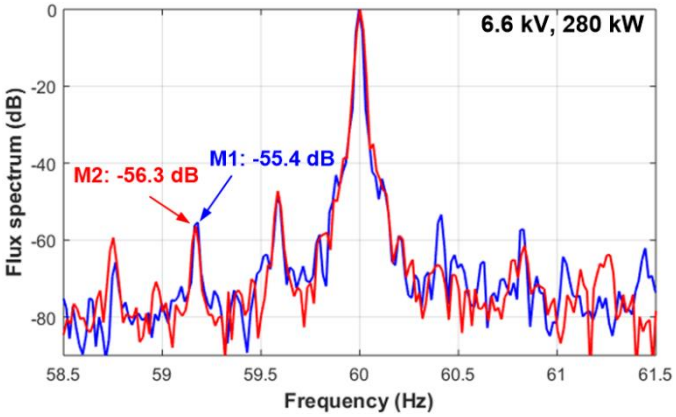

Fig. 16. Flux spectrum: (1-2*s*)f_s component for field motors: (a) with (M1: -52.5 dB MCSA) and (b) without (M2: <-70 dB MCSA) false positive rotor fault indication due axial air ducts

increase in the f_{rf} component is larger than 10 dB for all cases of broken bars for any given load or fault location. This clearly shows that flux monitoring provides sufficient sensitivity for reliable detection of rotor faults.

C. *Experimental Results – 6.6 kV, 280 kW Field Motor*

The results of the flux spectra obtained from the two identical 6.6 kV motors M1 and M2 (Fig. 1) with and without the false positive indications are shown in Fig. 16. The f_{rf} components in the flux spectra for M1 and M2 were -56.3 dB and -55.4 dB, respectively, for the motors that produced the -52.5 dB and <-70 dB f_{rf} components with MCSA (Fig. 4). It was smaller for M1 which produced a much larger f_{rf} component in the current. The difference in the amplitude of the f_{rf} components between the 2 motors was 0.9 dB in the flux spectra and larger than > 20 dB difference in the current spectra. This confirms that the axial air duct does not have a significant impact on the stray flux measurement. The amplitude of the inherent f_{rf} flux components are similar for M1 and M2, and also similar to that of the lab motor shown in Fig. 15. This component is expected to increase with rotor faults as in the case of Fig. 15, and therefore, is expected provide reliable detection of rotor faults immune to magnetic asymmetry, as claimed in IV.

VI. Conclusion

The reliability benefit of radial stray flux monitoring for detection of induction motors rotor cage faults was investigated in this paper. Although flux monitoring is simple and can be implemented with low cost, it has not received much attention as MCSA due to the lack of remote monitoring capability. This paper reports on the reliability aspect of flux monitoring for a case where MCSA fails due to magnetic asymmetry produced by axial cooling air ducts. This is known to be the most common cause of false MCSA rotor fault indication, and the main contribution of this work is to show that flux monitoring is immune to the axial duct influence for the first time. It was shown through experimental testing on lab and 6.6 kV field motors that flux monitoring is sensitive to rotor faults while being insensitive to the influence of axial ducts. It was clearly shown that radial stray flux monitoring is capable of providing

reliable detection of rotor faults for which MCSA fails to detect. Considering the advantages of flux monitoring, it is expected to be applied to critical industrial applications, where the reliability and sensitivity of fault detection outweighs the cost of installing flux coils.

REFERENCES

[1] A. Bellini, F. Filippetti, C. Tassoni, G.-A. Capolino, "Advances in Diagnostic Techniques for Induction Machines," *IEEE Trans. Ind. Electron.*, vol. 55, no. 12, pp. 4109-4126, Dec. 2008.

[2] M. Riera-Guasp, J.A. Antonino-Daviu, G.-A. Capolino, "Advances in Electrical Machine, Power Electronic, and Drive Condition Monitoring and Fault Detection: State of the Art," *IEEE Trans. Ind. Electron.*, vol. 62, no. 3, pp. 1746-1759, March 2015.

[3] R. de Jesus Romero-Troncoso, "Multirate Signal Processing to Improve FFT-Based Analysis for Detecting Faults in Induction Motors," *IEEE Trans. Ind. Informat.*, vol. 13, no. 3, pp. 1291-1300, June 2017.

[4] T.A. Garcia-Calva, D. Morinigo-Sotelo, R. de Jesus Romero-Troncoso, "Non-Uniform Time Resampling for Diagnosing Broken Rotor Bars in Inverter-Fed Induction Motors," *IEEE Trans. on Ind. Electron.*, vol. 64, no. 3, pp. 2306-2315, March 2017.

[5] G. Georgoulas *et al*., "The Use of a Multilabel Classification Framework for the Detection of Broken Bars and Mixed Eccentricity Faults Based on the Start-Up Transient," in *IEEE Trans. Ind. Informat.*, vol. 13, no. 2, pp. 625-634, April 2017.

[6] W.T. Thomson, and M. Fenger, "Current signature analysis to detect induction motor faults," *IEEE Ind. Appl. Mag.*, vol. 7, no. 4, pp. 26-34, July/Aug. 2001.

[7] W.T. Thomson, "On-line current monitoring – the influence of mechanical loads or a unique rotor design on the diagnosis of broken rotor bars in induction motors," *Proc. of ICEM*, pp. 1236-1240, 1992.

[8] B.D. Evans, "Induction motor case histories: a focus on electrically related phenomena," *Proc. of Vibration Institute Annual Meeting*, 2009.

[9] S.B. Lee, D. Hyun, T. Kang, C. Yang, S. Shin; H. Kim, S. Park, T. Kong, H. Kim, "Identification of false rotor fault indications produced by on-line MCSA for medium voltage induction machines," *IEEE Trans. Ind. Appl.*, vol. 52, no.1, pp. 729-738, Jan./Feb. 2016.

[10] A. Bellini, et al., "On-field experience with on-line diagnosis of large induction motors cage failures using MCSA," *IEEE Trans. Ind. Appl.*, pp. 1045-1053, vol. 38, no. 4, July/Aug. 2002.

[11] S. Lee, J. Hong, S.B. Lee, E. Wiedenbrug, M. Teska, and H. Kim, "Evaluation of the Influence of Rotor Axial Air Duct Design on Condition Monitoring of Induction Motors," *IEEE Trans. Ind. Appl.*, vol. 49, no. 5, pp.2024-2033, Sept./Oct. 2013.

[12] C. Yang et al. "Reliable Detection of Induction Motor Rotor Faults under the Rotor Axial Air Duct Influence," *IEEE Trans. on Ind. Appl.*, vol. 50, no. 4, pp. 2493-2502, July/Aug 2014.

[13] C. Yang *et al*., "Screening of False Induction Motor Fault Alarms Produced by Axial Air Ducts Based on the Space-Harmonic-Induced Current Components," *IEEE Trans. Ind. Electron.*, vol. 62, no. 3, pp. 1803-1813, March 2015.

[14] J. Penman, M.N. Dey, A.J. Tait, W.E. Bryan, "Condition monitoring of electrical drives," *IEE Proc. B – Elec. Pwr Appl.*, vol. 133, no. 3, pp. 142-148, May 1986.

[15] A. Ceban, R. Pusca, R. Romary, "Study of Rotor Faults in Induction Motors Using External Magnetic Field Analysis," *IEEE Trans. Ind. Electron.*, vol. 59, no. 5, pp. 2082-2093, May 2012.

[16] L. Frosini, C. Harlişca, L. Szabó, "Induction machine bearing fault detection by means of statistical processing of the stray flux measurement," *IEEE Trans. Ind. Electron.*, vol. 62, no. 3, pp. 1846-1854, Mar. 2015.

[17] A. Yazidi, H. Henao, G.-A. Capolino, "Broken rotor bars fault detection in squirrel cage induction machines," *IEEE IEMDC, pp. 741-747, May 2005*.

[18] C. Demian, A. Mpanda-Mabwe, H. Henao, G.-A. Capolino, "Detection of induction machines rotor faults at standstill using signals injection," *IEEE Trans. Ind. Appl.*, vol. 40, no. 6, pp. 1550-1559, Nov.-Dec. 2004.

[19] H. Henao, C. Demian, G.-A. Capolino, "A frequency-domain detection of stator winding faults in induction machines using an external flux sensor," *IEEE Trans. Ind. Appl.*, vol. 39, no. 5, pp. 1272-1279, Sept.-Oct. 2003.

[20] A. Bellini, C. Concari, G. Franceschini, C. Tassoni, A. Toscani, "Vibrations, currents and stray flux signals to asses induction motors rotor conditions," *Proc. of IEEE IECON*, pp. 4963-4968, 2006.

[21] N.M. Elkasabgy, A.R. Eastham, G.E. Dawson, "Detection of broken bars in the cage rotor on an induction machine," *IEEE Trans. Ind. Appl.*, vol. 28, no. 1, pp. 165-171, Jan./Feb. 1992.

[22] G.N. Surya, Z.J. Khan, M.S. Ballal, H.M. Suryawanshi, "A Simplified Frequency-Domain Detection of Stator Turn Fault in Squirrel-Cage Induction Motors Using an Observer Coil Technique," *IEEE Trans. Ind. Electron.*, vol. 64, no. 2, pp. 1495-1506, Feb. 2017.

[23] M. Irhoumah, R. Pusca, E. Lefevre, D. Mercier, R. Romary, C. Demian, "Information Fusion With Belief Functions for Detection of Interturn Short-Circuit Faults in Electrical Machines Using External Flux Sensors," *IEEE Trans. Ind. Electron.*, vol. 65, no. 3, pp. 2642-2652, March 2018.

[24] J. Antonino-Daviu, A. Quijano-López, V. Climente-Alarcon, H. Razik, "Evaluation of the detectability of rotor faults and eccentricities in induction motors via transient analysis of the stray flux," *Proc. of IEEE ECCE*, pp. 3559-3564, Oct. 2017.

[25] T. Goktas, M. Arkan, M.S. Mamis, B. Akin, "Separation of induction motor rotor faults and low frequency load oscillations through the radial leakage flux," *Proc. of IEEE ECCE*, pp. 3165-3170, Oct. 2107.

[26] T. Bishop, "Squirrel cage rotor testing," *EASA Convention*, 2003.

[27] C. Ammann, K. Reichert, R. Joho, Z. Posedel, "Shaft voltages in generators with static excitation systems-problems and solution," *IEEE Trans. Energy Convers.*, vol. 3, no. 2, pp. 409-419, Jun 1988.